Special Issue on "Theoretical and Computational Chemistry"

J. Indian Chem. Soc.,
Vol. 96, July 2019, pp. 1019-1028

Encapsulation of He clusters into carbon nanotubes: A modeling strategy based on continuum approximation and particle swarm optimization

Cheriyacheruvakkara Owais, Gopakumar Aswin and Rotti Srinivasamurthy Swathi*

School of Chemistry, Indian Institute of Science Education and Research Thiruvananthapuram (IISER-TVM), Vithura, Thiruvananthapuram-695 551, Kerala, India

E-mail: swathi@iisertvm.ac.in

Manuscript received online 13 May 2019, revised and accepted 03 June 2019

Theoretical investigations on the encapsulation of atoms and molecules into carbon nanotubes (CNTs) are dominated primarily by first-principles calculations, molecular dynamics and Monte Carlo simulations. Herein, we model the encapsulation of helium clusters, He_n (n = 2–10) into CNTs by employing the continuum approximation in conjunction with the particle swarm optimization technique implemented with the well-known local search strategy, limited memory Broyden-Fletcher-Goldfarb-Shanno algorithm. The endohedral as well as exohedral binding of the noble gas atoms in the vicinity of CNTs is driven by weak van der Waals interactions. The analysis enabled us to predict the equilibrium geometries of the clusters under confinement as well as the optimal CNT radii for the encapsulation of the clusters. We probed the effect of length of the CNTs in governing the energetics of encapsulation by considering semi-infinite CNTs and nanotubes of finite lengths (L = 10 Å, 20 Å, and 30 Å). The putative global minima structures obtained from our analysis can be employed as initial guesses for electronic structure calculations.

Keywords: Encapsulation, carbon nanotubes, helium clusters, continuum approach, particle swarm optimization.

Introduction

Atoms and molecules under confinement are known to exhibit fascinating properties and phenomena that are manifest as a consequence of the restriction in their geometries[1–5]. The emergence of carbon allotropes such as fullerenes, carbon nanotubes (CNTs) and graphene has kindled interest in researchers to investigate confinement effects within the hollow interior spaces of carbon nanotubes and fullerenes[6–18]. Studies on the encapsulation of atoms and molecules into CNTs have led to applications in drug delivery, gas storage, devices etc.[19–26]. Besides, confinement within the hollow cylindrical regions of the CNTs has also resulted in the emergence of novel optical signatures and new phases of matter[13,14,27–32]. Fullerenes enclosing atoms and molecules within their hollow spherical regions are referred to as endohedral fullerenes[33–35]. Successful synthesis of several endohedral fullerenes in recent years has provided a further impetus to research on confinement effects[36,37].

Numerous theoretical investigations have provided a fundamental understanding of the novel properties and phenomena arising out of confinement. Techniques such as first-principles approaches, molecular dynamics simulations and Monte Carlo simulations have been widely employed in various studies[9–14]. An accurate description of the energetics of encapsulation demands the use of first-principles approaches. However, one of the pertinent issues with regard to employing first-principles approaches for CNTs is the large system size. Since CNTs are not amenable to highly accurate first-principles calculations, alternative approaches such as semi-empirical methods that could provide meaningful estimates of the energetics at reasonable computational costs have become popular[38–40]. Researchers have attempted a variety of model potential descriptions for CNTs. One of the simple, yet powerful methodologies put forward in this direction is the continuum approximation[41–43]. Indeed, continuum approximation can be employed very effectively not just for CNTs but also for other highly symmetrical structures such as fullerenes and graphene. In continuum approximation, fullerenes, CNTs and graphene are modeled as systems with uniform density of carbon atoms on the surface of a sphere,

on the surface of a cylinder and in a planar region, respectively. The encapsulation of a single atom or a molecule into CNTs can be easily described by employing the continuum approximation[44–47]. However, modeling the encapsulation of a cluster of atoms or molecules into CNTs is rather complex owing to the possibility of several minima configurations on the potential energy surface (PES). Meta-heuristic population-based algorithms such as the particle swarm optimization (PSO) and genetic algorithm have become popular in recent times for describing the energetics of isolated clusters of atoms and molecules with several local minima[48–51]. Such global optimization techniques have been employed for estimating the energetics of the Lennard-Jones clusters, water clusters, benzene clusters, CO_2 clusters etc.[52–65].

In this work, we attempt to elucidate the energetics of the encapsulation of He clusters into CNTs by employing a unique strategy in which the CNTs are treated within the continuum approximation, while the He clusters are modeled using the PSO technique. The encapsulation of noble gases into CNTs has often been probed in the literature using first-principles calculations as well as molecular dynamics and Monte Carlo simulations[13,66,67]. We had earlier investigated the encapsulation of single noble gas atoms into CNTs by employing the continuum approximation and modeling the point-point interactions by the Lennard-Jones potential[47]. Herein, we consider the case of encapsulation of multiple He atoms into CNTs. The complexity arising due to the existence of several minima configurations on the PES is tackled by employing the PSO algorithm. Thus, the strategy of using the continuum approximation for CNTs in conjunction with the PSO for the atomic clusters enables us to decipher the energetics of the He cluster encapsulation into CNTs. The computational costs associated with such an approach are fairly reasonable and the resultant geometries for He clusters inside CNTs could serve as useful starting points for more accurate first-principles calculations. Besides, our strategy represents a significant step towards the modeling of encapsulation of several complex molecules into CNTs.

Methodology

The encapsulation of multiple He atoms, He_n (n = 2–10) into CNTs is driven by the weak van der Waals interactions. We employ the discrete-continuum model for describing the encapsulation of He clusters into CNTs. In the discrete-continuum model, a CNT is treated as a hollow cylinder with uniform surface density of carbon atoms and possessing a radius "*a*" whereas He clusters are considered as a collection of discrete atomic points. The interaction potential between a typical surface element on a CNT and a helium atom is described using the 6–12 Lennard-Jones potential[68] given by

$$V(\rho) = \frac{-A}{\rho^6} + \frac{B}{\rho^{12}} \quad (1)$$

where ρ is the distance between the surface element on the CNT and the helium atom, and A and B are the Lennard-Jones attractive and repulsive constants, respectively. The total energy is obtained by integrating the interaction term between a surface element and a gas atom over the entire surface of the CNT. We get the total interaction energy between a He cluster and a CNT by adding the contributions from the interactions of all the helium atoms. We analyze the encapsulation of multiple He atoms, He_n (n = 2–10) into CNTs using two approaches. In the first (approach 1), we arrive at the optimal geometries of He clusters within CNTs and the optimal CNT radii for encapsulation by optimizing the separations between noble gas atoms. In the second (approach 2), we first optimize the geometries of the gas phase He clusters and the rigid clusters are then encapsulated into CNTs to determine the optimal radii of CNTs for the encapsulation of the clusters. The optimization is performed using PSO, a global search technique by incorporating a local search technique for better exploitation of the PES. In each optimization, the putative global minima structure is obtained from ~100 simulation sample configurations.

Approach 1: Encapsulation of helium clusters into CNTs

We first arrive at the optimal geometries of He clusters within CNTs and the optimal CNT radii for encapsulation by optimizing the separations between noble gas atoms. The position of each helium atom with respect to a CNT can be described using three cartesian coordinates (x,y,z) as illustrated in Fig. 1.

The total interaction energy that accounts for all the non-covalent interactions is obtained by adding the energies of

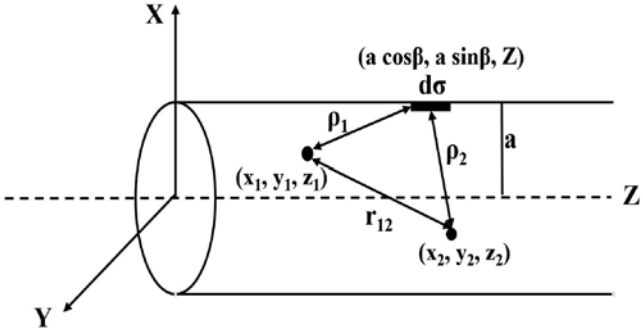

Fig. 1. A schematic illustrating the key parameters in the discrete-continuum model for the interaction between a semi-infinite CNT and two He atoms.

interaction (i) between the helium atoms and (ii) between the helium atoms and the CNT as given by

$$E_{\text{total}} = \sum_{i=1}^{N-1} \sum_{j=i+1}^{N} \left(\frac{-A_{ij}}{r_{ij}^{6}} + \frac{B_{ij}}{r_{ij}^{12}} \right)$$

$$+ \sum_{i=1}^{N} n_g \int \left(\frac{-A_i}{\rho_i^{6}} + \frac{B_i}{\rho_i^{12}} \right) d\sigma \qquad (2)$$

where N is the number of helium atoms, $r_{ij} = [(x_i - x_j)^2 + (y_i - y_j)^2 + (z_i - z_j)^2]^{1/2}$ is the distance between i-th and j-th helium atoms and $\rho_i = [(x_i - a\cos\beta)^2 + (y_i - a\sin\beta)^2 + (z_i - Z)^2]^{1/2}$ is the distance between i-th helium atom and a tiny surface element $d\sigma$ on the CNT. n_g is the atomic surface density of the CNT. The second term in eq. (2) can be written as

$$E_2 = \sum_{i=1}^{N} a n_g \left(-A_i J_3^i + B_i J_6^i \right) \qquad (3)$$

where J_n^i is defined by

$$J_n^i = \int_0^L \int_0^{2\pi} \frac{1}{\rho_i^{2n}} d\beta dZ \qquad (4)$$

with $n = 3$ and $n = 6$ and L is the length of the CNT. In case of semi-infinite CNTs, $L = \infty$. Thus, the total binding energy, defined as the negative of E_{total} includes the contributions from He-He as well as He-C interactions.

Approach 2: Encapsulation of helium clusters into CNTs

In the next approach, the optimized helium clusters are considered as rigid bodies with fixed internal coordinates. The relative positions of the helium atoms in a cluster with respect to a CNT are given by the cartesian coordinates (x,y,z) as illustrated in Fig. 2.

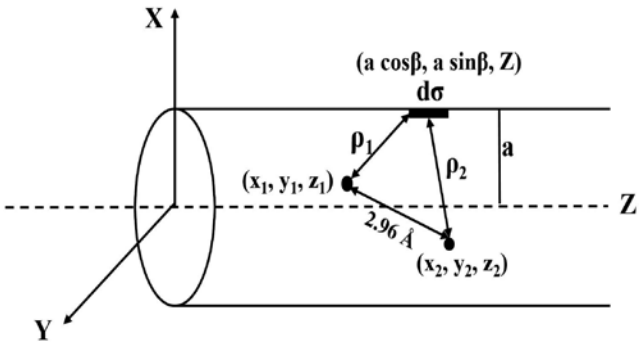

Fig. 2. A schematic illustrating the key parameters in the discrete-continuum model for the interaction between a semi-infinite CNT and a rigid He_2 cluster.

The total interaction energy between a CNT and a helium cluster is obtained by summing the contributions of the interaction energies of each helium atom with the CNT and is given by

$$E_{\text{tot}} = \sum_{i=1}^{N} n_g \int \left(\frac{-A_i}{\rho_i^{6}} + \frac{B_i}{\rho_i^{12}} \right) d\sigma \qquad (5)$$

where N is the number of helium atoms in the cluster and $\rho_i = [(x_i - a\cos\beta)^2 + (y_i - a\sin\beta)^2 + (z_i - Z)^2]^{1/2}$ is the distance between i-th helium atom and a tiny surface element $d\sigma$ on the CNT. The above equation for total interaction energy can be written as

$$E_{\text{tot}} = \sum_{i=1}^{N} a n_g \left(-A_i I_3^i + B_i I_6^i \right) \qquad (6)$$

where I_n^i is defined by

$$I_n^i = \int_0^L \int_0^{2\pi} \frac{1}{\rho_i^{2n}} d\beta dZ \,. \qquad (7)$$

Since the energy term E_{tot} includes only the He-C interactions and the cluster geometries are kept rigid in this approach, the binding energy evaluated as the negative of E_{tot} includes the contributions from the He-C interactions only. The center of the opening of the CNT is taken as the origin of the laboratory-fixed frame. The position of the center of mass of the helium cluster is represented in the laboratory-fixed

frame. The orientation of the helium cluster inside the CNT is described by using the Euler angles (θ, ψ, φ). The position ($\boldsymbol{r}_i^{LAB}$) of atom i in the cluster with respect to the lab frame can be expressed in terms of the corresponding center of mass coordinate ($\boldsymbol{r}^{LAB}$) expressed in laboratory frame and body-fixed position ($\boldsymbol{r}_i^{BF}$) of atom i in the cluster as

$$\boldsymbol{r}_i^{LAB} = \boldsymbol{r}^{LAB} + R^{-1}(\theta, \psi, \varphi)\, \boldsymbol{r}_i^{BF} \tag{8}$$

where R^{-1} is the inverse of the Euler rotation matrix.

Particle swarm optimization

PSO is a stochastic global search technique inspired by social behaviours such as fish schooling and bird flocking[48]. It is a population-based method with population size K, where the coordinate of each particle in the swarm represents a potential solution for the objective function i.e. function to be minimized. In PSO, at each iteration, the candidate solution also called particles moves through the search space in search of global optima by improving the quality of the solution. Each particle in the swarm has a position and a velocity. In each iteration of the algorithm, velocity, followed by position, is updated for every particle to get the best solution and fitness value (negative of the function value for minimization problems) using the current population. Particles store their best solution in memory known as personal best (*pbest*) and the best position achieved by any particle in the iterations is called the global best (*gbest*). Each particle, i in the population is represented using a D-dimensional vector

$$X_i = [X_i^1, X_i^2, ..., X_i^D].\ i = 1, ..., K.$$

The initial velocity of each particle is randomly generated and is represented as

$$V_i = [V_i^1, V_i^2, ..., V_i^D].$$

In a given iteration, each particle updates its velocity and position using the equations below:

$$V_i^{(t+1)} = V_i^{(t)} + c_1 r_1 \left(pbest_i^{(t)} - X_i^{(t)}\right) + c_2 r_2 \left(gbest^{(t)} - X_i^{(t)}\right) \tag{9}$$

$$X_i^{(t+1)} = X_i^{(t)} + V_i^{(t+1)} \tag{10}$$

where c_1 and c_2 are the cognitive and the social acceleration constants. r_1 and r_2 are random vectors generated from a uniform distribution belonging to the interval [0,1], $pbest_i^{(t)}$ is the position of the particle i where the function has achieved its minimum on or before time t and $gbest^{(t)}$ is the best solution that the swarm has achieved at time t. We employ the limited memory Broyden-Fletcher-Goldfarb-Shanno (L-BFGS) local optimization technique in the PSO algorithm. The algorithm is depicted in Fig. 3.

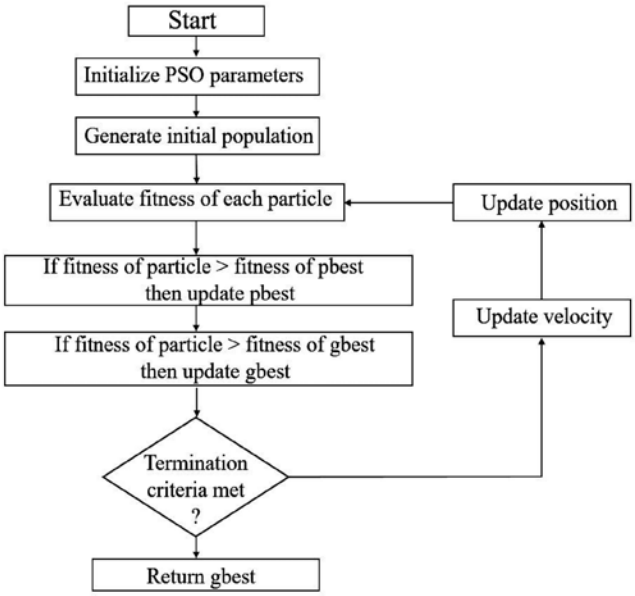

Fig. 3. PSO algorithm.

Results and discussion

We have performed the global optimization of the interaction energies of a series of He clusters with CNTs as a function of CNT length as well as CNT radius by employing the PSO algorithm with the L-BFGS local optimization technique using Maple[70]. In this study, an initial guess for the particle in the PSO algorithm corresponds to a configuration of isolated He atoms or He-CNT system. For the optimization of isolated helium clusters, the initial guess for the particle is designed by placing the He atoms at random positions within a cutoff distance for possible interactions. For the He-CNT system, the positions of the helium atoms are constrained to be within the CNTs. In approach 1, the helium atoms are randomly placed inside the CNTs. Thus, at the initial point, the two particles are completely unrelated and to get the configuration of another particle, every He atom has to be translated. While in the second approach, initial guess for each particle is correlated by translation and rotation along the center of mass of the rigid He cluster. The parameters used in the calculations are given in Table 1.

Table 1. Numerical values of various parameters employed in the calculations

Parameters	Numerical values
Atomic surface density of CNTs[44]	0.3812 atoms/Å^2
He-He attractive constant, A_{He-He}[69]	0.6377 eV×Å^6
He-He repulsive constant, B_{He-He}[69]	215.8916 eV×Å^{12}
He-C attractive constant, A_{He-C}[43]	3.5045 eV×Å^6
He-C repulsive constant, B_{He-C}[43]	2774.8849 eV×Å^{12}

Initially, we investigated the confinement of helium clusters inside CNTs using approach 1. We carried out this analysis for CNTs of lengths L = 10 Å, 20 Å, 30 Å and for semi-infinite CNTs to understand the changes in equilibrium geometries of clusters as a function of the length of the CNTs. For finding the equilibrium geometries as well as the optimal CNT radii for encapsulation, we randomly initialize the positions of helium atoms inside the CNTs. The design variables for optimization include the position vectors of all the helium atoms and the radius of the CNT. In order to confine the helium atoms within the CNTs, we used a penalty function such that the moment any helium atom goes outside the CNT wall during the simulation, its contribution to the total interaction energy is set to a very high positive value. The total binding energy includes the contributions from He-He interactions and He-C interactions. The binding energy contributions from both the interactions are given in Supplementary Information (see Tables SIV, SVI, SVIII and SX). The contributions from He-He interactions are found to be very small when compared to the He-C interactions. In the optimized geometries of the clusters encapsulated into CNTs of length 30 Å and into semi-infinite CNTs (Tables SVII and SIX of Supplementary Information), all the helium atoms are found to be on the CNT axes with a van der Waals distance of ~2.85–2.95 Å between the adjacent helium atoms. The optimal radius for the encapsulation of He into the semi-infinite CNTs is found to be 3.30 Å for all the clusters. However, in case of short CNTs of lengths 10 Å and 20 Å (Tables SIII and SV of Supplementary Information), we notice deviations from the linear cluster geometries for larger He clusters. A comparison of the optimal CNT radii and binding energies obtained for the confinement of the helium clusters into CNTs of various lengths is shown in Fig. 4.

When the length of the CNT is decreased, the helium atoms do not necessarily form a chain of atoms along the axes of the CNTs. For example, in the case of CNT with L =

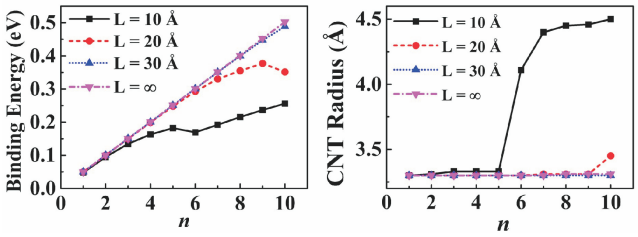

Fig. 4. Binding energies and optimal radii for the encapsulation of helium atoms into CNTs of lengths, L = 10 Å, 20 Å and 30 Å, and semi-infinite CNTs.

10 Å, up to the encapsulation of three helium atoms, the binding energy values are found to be similar to the values obtained in the semi-infinite case. However, there is a notable variation in binding energy values for the encapsulation of four He atoms (Fig. 4). Thus, it can be inferred that the addition of four or more He atoms to CNTs of L = 10 Å is not favorable since the largest binding energies are obtained for the semi-infinite case. However, helium atoms still prefer to lie on the CNT axes up to the n = 5 cluster with a decreased separation between adjacent He atoms. The trends obtained in Fig. 4 indicate that the encapsulation of He_n (n = 2–10) clusters into reasonably large CNTs (CNTs of length 30 Å and semi-infinite CNTs) is very facile. Due to confinement effects, the minima obtained in the case of short CNTs may or may not be the global minima. As a result, the search space has to be extended for finding the global minima outside the CNT wall as well.

We have further extended the search space by 4 Å in both X and Y directions outside the CNTs in order to see whether there are any other configurations with binding energies higher than those found for the preferred configurations on confinement. The binding energies obtained in the following three He-CNT clusters are found to be higher when the confinement condition is relaxed: (i) interaction of six He atoms with a CNT of length L = 10 Å, (ii) interaction of seven He atoms with a CNT of length L = 10 Å and (iii) interaction of ten He atoms with a CNT of length L = 20 Å. Interestingly, one, two and one helium atoms, respectively in the above three cases are found to bind at exohedral positions for these clusters and the exohedral atoms are found to lie at a distance of ~3 Å distance from the CNT wall. The optimal CNT radii for all the three clusters is found to be 3.30 Å and the average binding energy per atom is estimated to be ~0.05 eV. Such configurations found without the constraints of con-

finement can be considered as the global minima for interaction with short CNTs since the binding energies are higher than the cases when all the He atoms are confined within the CNTs. The success rate of the algorithm depends on the dimensionality of the potential energy function and the search space. As the number of He atoms increases, the dimensionality of the potential energy function increases and hence the success rate decreases. In cases where the confinement condition is not employed, extending the search space outside the CNT without chemical intuition or trial runs can substantially decrease the success rate.

We have also analyzed the variation in binding energies as well as equilibrium geometries with respect to the CNT radius for the encapsulation of helium clusters into CNTs of lengths L = 10 Å, 20 Å, 30 Å and for semi-infinite CNTs. When the CNT radius is very small, it is unfavourable for the helium atoms to bind endohedrally within the CNTs. From Fig. 5, we note that the binding energies initially increase with the increase in CNT radius. Subsequently, the energy

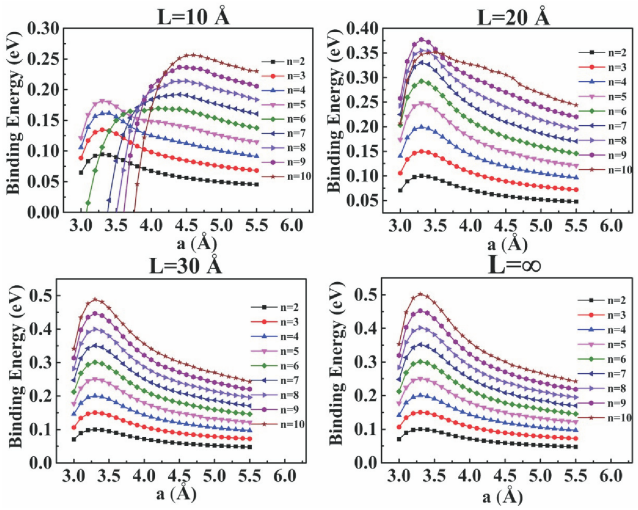

Fig. 5. The variation in binding energies as a function of the CNT radius for the encapsulation of helium clusters into CNTs of various lengths.

values decrease monotonically with the increase in CNT radius and the helium atoms move away from the CNT axes to one of the walls of the CNT in order to maximize the binding energies. The length of the CNT plays a major role in governing the binding energies as well as the equilibrium geometries. The binding energies of course increase when the number of helium atoms in the cluster increases.

The continuum description of CNTs has enabled us to assess the energetics of encapsulation at reasonable computational costs. We now shed some light on the accuracy of such a continuum description when compared to an explicit atomistic description of CNTs. We have performed further calculations based on the discrete model with atomistic representations for various CNTs. We have used atomistic models of CNTs of chiral indices (8,1), (6,4), (10,1), (7,6), (8,5) and (11,1) with radii 3.31 Å, 3.45 Å, 4.12 Å, 4.41 Å, 4.45 Å and 4.51 Å respectively. In the case of (8,1) CNT, CNT lengths of L = 10 Å, 20 Å and 30 Å are considered. For CNTs of other chiral indices, we have considered CNTs of length L = 10 Å. All molecular model structures of CNTs for the discrete model calculations are generated using the Avogadro software[71]. The CNT geometries are kept rigid during the discrete model calculations. A comparison of the binding energies obtained based on the discrete model calculations and the discrete-continuum model calculations for CNTs of various lengths is shown in Fig. 6. The optimized geometries for the encapsulation of various He clusters into CNTs of length L = 10 Å are

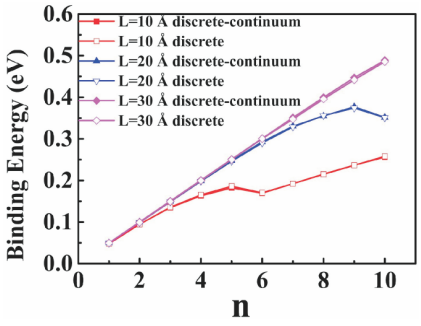

Fig. 6. A comparison of the binding energies from the discrete and the discrete-continuum approaches for the encapsulation of He clusters into CNTs of various lengths.

given in Fig. 7. The computed binding energies from the discrete representation of CNTs and the discrete-continuum approach show a good quantitative agreement (Fig. 6). We however note that the discrete-continuum approach is computationally very cheap in comparison with the discrete approach for describing the properties of He-CNT clusters and is thus the suggested method for such analysis.

We have also considered the case of very large CNT radius (i.e. a $\rightarrow \infty$) wherein the binding energies for the en-

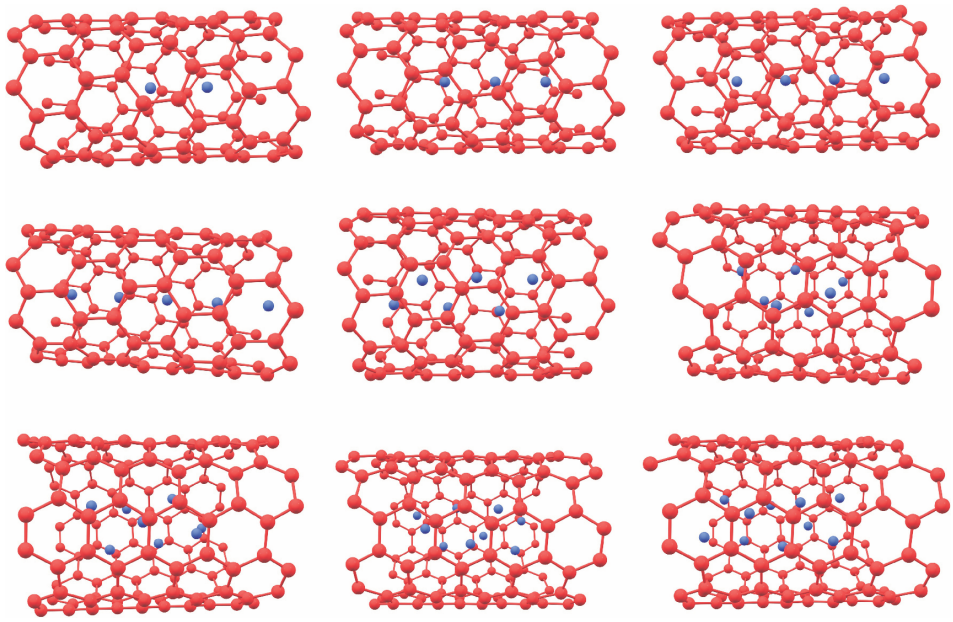

Fig. 7. The optimized geometries for the encapsulation of He clusters (n = 2–10) into various CNTs of length, L = 10 Å. The chiral indices for the CNTs used are: (8,1) CNT for n = 2–5, (10,1) CNT for n = 6, (8,5) CNT for n = 7 and 8, (7,6) CNT for n = 9 and (11,1) CNT for n = 10.

capsulation of helium atoms are expected to converge to the graphene limit. The binding energies thus obtained are to be interpreted as the adsorption energies for the clusters on graphene. From Fig. 5, it is clear that the binding energies start to decrease with increase in CNT radius on reaching the optimal CNT radius. A comparison of the computed binding energies for CNTs of length, L = 10 Å, 20 Å, 30 Å and for semi-infinite CNTs in the graphene limit is shown in Fig. 8 (and Table SXV of Supplementary Information). The binding energies obtained in the graphene limit increase with the increase in the number of He atoms as well as with the length

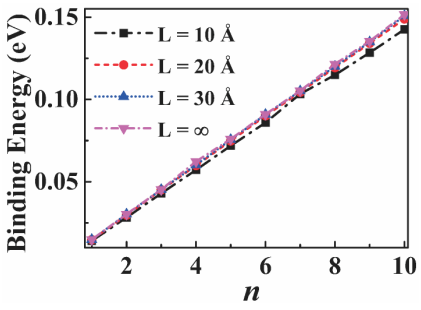

Fig. 8. Binding energies as a function of the cluster size for the encapsulation of He clusters into CNTs of large radii (graphene limit).

of the nanotube. However, the binding energies are found to converge after a length of L = 30 Å. Thus, CNTs of length L = 30 Å could be ideal starting points for probing the energetics of encapsulation into CNTs using electronic structure methods. On optimization, we note that all the helium atoms are located at a distance of ~3.05 Å from the CNT wall, which corresponds to the physisorption distance of He on graphene.

Finally, we analyze the conditions under which isolated He clusters could be encapsulated into CNTs with retention of geometries (approach 2). We determine the radii of the CNTs for which the rigid helium clusters bind strongly with the CNTs. The bare helium clusters, He_n (n = 2–10) are initially optimized using the PSO algorithm. The energy minima and the optimized geometries and coordinates of the He atoms thus obtained for various clusters are given in Supplementary Information (see Tables SI and SII and Fig. S1). The design variables for optimization in case of the analysis of the rigid He cluster encapsulation into CNTs are the center of mass of the cluster with respect to the lab frame (X, Y, Z) and the Euler angles (θ, ψ, φ). The trends in binding energies, as well as the optimal CNT radii for the encapsulation of the rigid helium clusters into CNTs are shown in Fig. 9. Due to the difference in symmetries of the bare helium

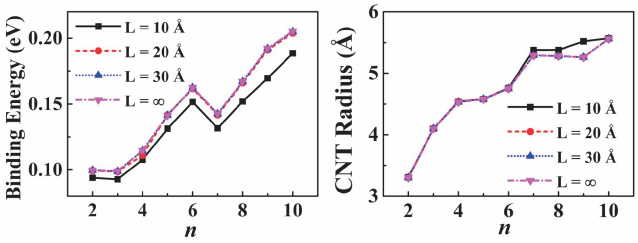

Fig. 9. Binding energies and optimal CNT radii for the encapsulation of the rigid helium clusters, He_n (n = 2–10) into CNTs of various lengths.

clusters, we do not find a strict correlation between the optimal CNT radii, binding energies and the number of helium atoms in the cluster. The lowering of the binding energies for the encapsulation of rigid helium clusters when compared to the previous case wherein the helium atom coordinates were allowed to vary, clearly indicates that the retention of isolated cluster geometries on encapsulation is not energetically favorable. The coordinates of helium atoms in the equilibrium geometries found on rigid cluster encapsulation are given in Supplementary Information (see Tables SXI–SXIV). Finally, we comment on some generic aspects of the adopted methodology for investigating encapsulation. Encapsulation, in general, does not necessarily occur spontaneously and is dictated by thermodynamic as well as kinetic requirements. For spontaneous encapsulation, the thermodynamic requirement of free energy decrease on encapsulation and the kinetic requirement of non-existence of repulsive barriers at the CNT openings have to be met. If the energy barrier for passage is zero, the encapsulation is facile. If the barrier is non-zero but small, the encapsulation can be facilitated by the additional kinetic energy of the incoming species. However, if the repulsive barrier is large, the encapsulation process is non-spontaneous. The consequences of not considering free energy as a metric are not very significant in case of the encapsulation of noble gas atoms into CNTs. The binding free energies typically comprise enthalpic and entropic contributions. The encapsulation of noble gases is driven by the van der Waals interactions between the He atoms and the CNTs. The enthalpic contributions are much higher in comparison with the entropic contributions and the binding free energies are primarily governed by the enthalpic contributions. Our analysis of the interaction energies includes the van der Waals interactions, which make a predominant contribution to the enthalpic changes. We note here that, for CNT-noble gas systems, electrostatic contributions are minimal. It is of course possible to estimate the binding free energies by assessing the enthalpic as well as entropic contributions by performing molecular dynamics simulations.

Conclusions

We have employed the continuum approximation and the particle swarm optimization technique to probe the encapsulation of helium clusters, He_n (n = 2–10) into CNTs for varying CNT lengths and radii. Semi-infinite CNTs possessing a radius of 3.30 Å yield the largest binding energies for the encapsulation of the investigated He clusters. In case of encapsulation of rigid He clusters in their isolated cluster geometries into CNTs, we noted lowering of the binding energies compared to the case when the separations between the He atoms are optimized, indicating that such configurations are unfavorable. In the limit of large CNT radii, the computed binding energies lead to the adsorption energies of clusters on graphene. The efficiency of the employed algorithm depends on the dimensionality of the potential energy function as well as the extent of the search space. We also extended the search space beyond the interior of the CNTs to probe the exohedral binding of the He atoms on the CNTs thereby obtaining the putative global minima structures. The approach presented herein can be extended to describe the encapsulation of complex atomic or molecular clusters possessing a large number of atoms by incorporating the PSO variants that can bypass the problems associated with dimensionality.

Acknowledgements

The authors thank Anto James for providing feedback by a careful reading of the manuscript. The authors also acknowledge IISER-TVM for computational facilities. RSS acknowledges the Kerala State Council for Science, Technology and Environment (KSCSTE) for financial support of this work, through the grant number KSCSTE/430/2018-KSYSA-RG. CHO thanks IISER-TVM for the fellowship. GA is grateful to the Department of Science and Technology, Government of India for the INSPIRE fellowship.

Supporting Information

Supplementary figures and tables are provided in the Supporting Information.

References

1. F. J. Keil, R. Krishna and M. Coppens, *Rev. Chem. Eng.*, 2011, **16**, 71.
2. M. E. Davis, *Ind. Eng. Chem. Res.,* 1991, **30**, 1675.
3. M. F. Zalazar, E. N. Paredes, G. D. R. Ojeda, N. D. Cabral and N. M. Peruchena, *J. Phys. Chem. C*, 2018, **122**, 3350.
4. M. F. Zalazar, N. D. Cabral, G. D. R. Ojeda, C. I. A. Alegre and N. M. Peruchena, *J. Phys. Chem. C,* 2018, **122**, 27350.
5. R. Gounder and E. Iglesia, *Chem. Commun.,* 2013, **49**, 3491.
6. J. Xiao, X. Pan, F. Zhang, H. Li and X. Bao, *Chem. Sci.,* 2017, **8**, 278.
7. W. Chen, Z. Fan, L. Gu, X. Baoc and C. Wang, *Chem. Commun.,* 2010, **46**, 3905.
8. Y. Li, W. Lu, H. Fu, X. Zhao and S. Xu, *Nanotechnology,* 2017, **28**, 425604 (1-8).
9. Y. Liu, R. O. Jones, X. L. Zhao and Y. Ando, *Phys. Rev. B,* 2003, **68**, 125413 (1-7).
10. Y. J. Dappe, *J. Phys. D: Appl. Phys.,* 2014, **47**, 083001 (1-16).
11. L. Tang and X. Yang, *J. Phys. Chem. C,* 2012, **116**, 11783.
12. J. Hernandez-Rojas, F. Calvo, J. Breton and J. M. Gomez Llorente, *J. Phys. Chem. C,* 2012, **116**, 17019.
13. M. K. Agusta, I. Prasetiyo, A. G. Saputro, R. Maezono and H. K. Dipojono, *J. Phys.: Conf. Ser.,* 2016, **739**, 012081 (1-7).
14. D. Chakraborty and P. K. Chattaraj, *Chem. Phys. Lett.,* 2015, **621**, 29.
15. N. Naguib, H. Ye, Y. Gogotsi, A. G. Yazicioglu, C. M. Megaridis and C. M. Yoshimura, *Nano Lett.,* 2004, **4**, 425604.
16. Z. Liu, K. Yanagi, K. Suenaga, H. Kataura and S. Iijima, *Nat. Nanotechnol.,* 2007, **32**, 422.
17. Y. Zoua, B. Liua, L. Wanga, D. Liua, S. Yua, P. Wanga, T. Wanga, M. Yaoa, Q. Lia and B. Zoua, *PNAS,* 2009, **106**, 22135.
18. M. Y. Amusia, A. S. Baltenkov and U. Becker, *Phys. Rev. A,* 2000, **62**, 012701 (1-4).
19. J. Y. Chen, S. Y. Chen, X. R. Zhao, L. V. Kuznetsova, S. S. Wong and I. Ojima, *J. Am. Chem. Soc.,* 2008, **130**, 16778.
20. C. H. Wu, C. Cao, J. H. Kim, C. H. Hsu, H. J. Wanebo, W. D. Bowen, J. Xu and J. Marshall *Nano Lett.,* 2012, **12**, 5475.
21. W. X. Zhang, Z. Z. Zhang and Y. G. Zhang, *Nanoscale Res. Lett.,* 2011, **6**, 555 (1-22).
22. J. J. Zhao, A. Buldum, J. Han and J. P. Lu, *Nanotechnology,* 2002, **13**, 195.
23. S. Santucci, S. Picozzi, F. Di Gregorio, L. Lozzi, C. Cantalini, L. Valentini, J. M. Kenny and B. Delley, *J. Chem. Phys.,* 2003, **119**, 10904.
24. G. E. Froudakis, *Mater. Today,* 2011, **14**, 324.
25. D. Lu, Y. Li, U. Ravaioli and K. Schulten, *Phys. Rev. Lett.,* 2005, **95**, 246801 (1-4).
26. Q. Zheng and Q. Jiang, *Phys. Rev. Lett.,* 2002, **88**, 045503 (1-3).
27. D. V. Kazachkin, Y. Nishimura, H. A. Witek, S. Irle and E. Borguet, *J. Am. Chem. Soc.,* 2011, **133**, 8191.
28. A. W. Hauser and M. P. de Lara-Castells, *J. Phys. Chem. Lett.,* 2016, **7**, 4929.
29. A. Noury, J. Vergara-Cruz, P. Morfin, B. Placais, M. C. Gordillo, J. Boronat, S. Balibar and A. Bachtold, *Phys. Rev. Lett.,* 2019, **122**, 165301 (1-6).
30. F. Z. Cui, J. Ma, D. Y. Huo and Z. J. Chen, *Phys. Lett. A,* 2004, **332**, 417.
31. M. Abbaspouri, H. Akbarzadeh, S. Z. Banihashemi and A. Sotoudeh, *Physica A,* 2018, **491**, 219.
32. A. W. Hauser, A. O. Mitrushchenkov and M. P. de Lara-Castells, *J. Phys. Chem. C,* 2017, **121**, 3807.
33. A. A. Popov, S. Yang and L. Dunsch, *Chem. Rev.,* 2013, **113**, 5989.
34. S. Yang, T. Wei and F. Jin, *Chem. Soc. Rev.,* 2017, **46**, 5005.
35. T. Nakane, Z. Xu, E. Yamamoto, T. Sugai, T. Tomiyama and H. Shinohara, *Fullerene Sci. Technol.,* 1997, **5**, 829.
36. M. d. C. Gimenez-Lopez, A. Chuvilin, U. Kaiser and A. N. Khlobystov, *Chem. Commun.,* 2011, **47**, 2116.
37. R. B. Ross, C. M. Cardona, D. M. Guldi, S. G. Sankaranarayanan, M. O. Reese, N. Kopidakis, J. Peet, B. Walker, G. C. Bazan and E. V. Keuren, *Nat. Mater.,* 2009, **8**, 208.
38. F. Pirani, S. Brizi, L. F. Roncaratti, P. Casavecchia, D. Cappelletti and F. Vecchiocattivi, *Phys. Chem. Chem. Phys.,* 2008, **10**, 5489.
39. F. Pirani, M. Albert, A. Castro, M. M. Teixidor and D. Cappelletti, *Chem. Phys. Lett.,* 2004, **394**, 37.
40. M. Bartolomei, E. Carmona-Novillo, M. I. Hernndez, J. Campos-Martnez and F. Pirani, *J. Phys. Chem. C,* 2013, **117**, 10512.
41. B. J. Cox, N. Thamwattana and J. M. Hill, *Proc. R. Soc. A,* 2007, **463**, 461.
42. B. J. Cox, N. Thamwattana and J. M. Hill, *Proc. R. Soc. A,* 2007, **463**, 477.
43. T. A. Hilder and J. M. Hill, *J. Phys. A: Math. Theor.,* 2007, **40**, 3851.
44. T. Tran-Duc, N. Thamwattana, B. J. Cox and J. M. Hill, *Comput. Mater. Sci.,* 2011, **50**, 2720.
45. T. Tran-Duc, N. Thamwattana and J. M. Hill, *J. Math. Chem.,* 2011, **49**, 1115.
46. M. H. Alshehri, B. J. Cox and J. M. Hill, *Micro Nano Lett.,* 2013, **9**, 113.
47. S. G. Balasubramani, D. Singh and R. S. Swathi, *J. Chem. Phys.,* 2014, **141**, 184304 (1-15).

48. J. Kennedy and R. Eberhart, *Proc. IEEE Int. Conf. Neural Netw.,* 1995, **4**, 1942.
49. J. H. Holland, "Adaptation in Natural and Artificial Systems", 2nd ed., University of Michigan Press, Ann Arbor, MI, 1975, 1992.
50. A. K. Qin, V. L. Huang and P. N. Suganthan, *IEEE Trans. Evol. Comput.,* 2009, **13**, 398.
51. X.-S. Yang and A. H. Gandomi, *Eng. Computation,* 2012, **29**, 464.
52. A. O. Lyakhova, A. R. Oganova, H. T. Stokes and Q. Zhu, *Comput. Phys. Commun.,* 2013, **184**, 1172.
53. D. J. Wales and H. A. Scheraga, *Science,* 1999, **285**, 1368.
54. C. Barron, S. Gomez, D. Romero and A. Saavedra, *Appl. Math. Lett.,* 1999, **12**, 85.
55. T. Lazauskas, A. A. Sokol and S. M. Woodley, *Nanoscale,* 2017, **9**, 3850.
56. W. J. Pullan, *J. Chem. Inf. Comput. Sci.,*1997, **37**, 1189.
57. H. Takeuchi, *J. Phys. Chem. A,* 2008, **112**, 7492.
58. J. L. Llanio-Trujillo, J. M. C. Marque and F. B. Pereira, *J. Phys. Chem. A,* 2011, **115**, 2130.
59. J. M. C. Marques, F. B. Pereira, J. L. Llanio-Trujillo, P. E. Abreu, M. Alberti, A. Aguilar, F. Pirani and M. A Bartolomei, *Phil. Trans. R. Soc. A,* 2017, **375**, 20160198 (1-17).
60. B. S. Gonzalez, J. Hernandez- Rojas and D. J. Wales, *Chem. Phys. Lett.,* 2005, **412**, 23.
61. C. K. N. Marcus, S. Fong and S. W. I. Siu, *J. Bioinform. Comput. Biol.,* 2015, **13**, 1541007 (1-18).
62. Y. Wang, M. Miao, J. Lv, L. Zhu, K. Yin, H. Liu and Y. Ma, *J. Chem. Phys.,* 2012, **137**, 224108 (1-6).
63. Y. Wang, J. Lv, L. Zhu and Y. Ma, *Phys. Rev. B,* 2010, ***82***, 094116 (1-8).
64. S. T. Call, D. Y. Zubarev and A. I. Boldyrev, *J. Comput. Chem.,* 2006, **28**, 1177.
65. K. K. Bejagam, S. Singh and S. A. Deshmukh, *J. Comput. Chem.,* 2018, **39**, 721.
66. R. Majidi, *Fullerene Nanotubes Carbon Nanostruct.,* 2014, **22**, 520.
67. H. Sha and R. Faller, *Comput. Mater. Sci.,* 2016, **114**, 160.
68. J. E. Lennard-Jones, *Proc. Phys. Soc.,* 1931, **43**, 461.
69. C. John and R. S. Swathi, Unpublished, 2019.
70. Maple 17. Maplesoft: Waterloo ON, Canada, 2017.
71. M. D. Hanwell, D. E. Curtis, D. C. Lonie, T. Vandermeersch, E. Zurek and G. R. Hutchison, *J. Cheminf.,* 2012, **4**, 17 (1-17).